JPCCCK

VOLUME 112
JULY 24, 2008
NUMBER 29

http://pubs.acs.org/JPCC

THE JOURNAL OF PHYSICAL CHEMISTRY C

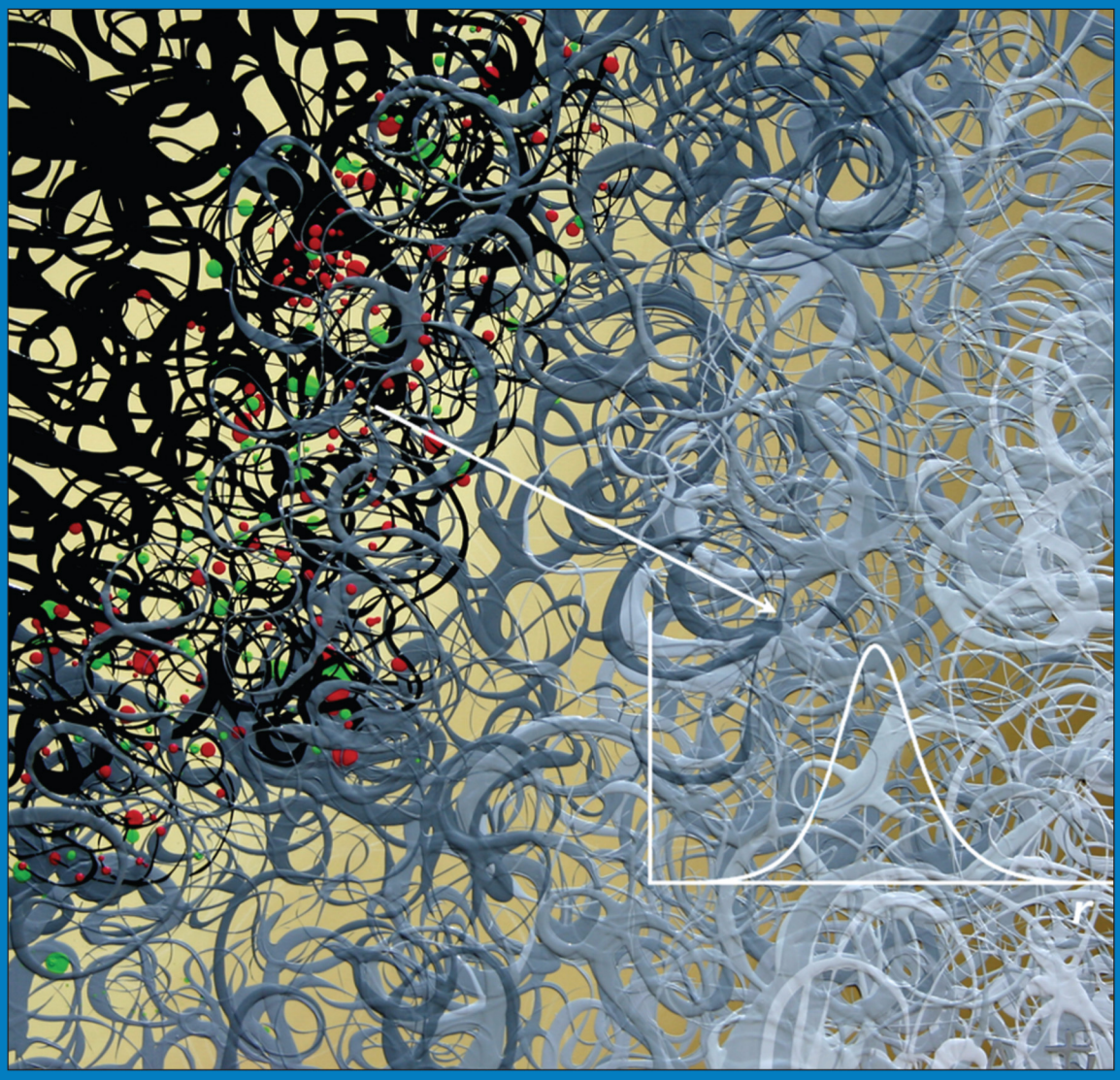

Resonance Energy Transfer Between Dyes in Nanosized Domains at Polymer Interfaces
(see page 7A)

NANOMATERIALS, INTERFACES, HARD MATTER

PUBLISHED WEEKLY BY THE AMERICAN CHEMICAL SOCIETY

REVIEW ARTICLE

Resonance Energy Transfer in Polymer Nanodomains

J. P. S. Farinha* and J. M. G. Martinho

Centro de Química-Física Molecular and IN—Institute of Nanoscience and Nanotechnology, Instituto Superior Técnico, 1049-001 Lisboa, Portugal

Received: February 25, 2008; Revised Manuscript Received: May 05, 2008

The properties of nanostructured polymer materials are often determined by their interfacial domains, which are typically 1−10 nm thick. This range matches the length scale of Förster resonance energy transfer (FRET). While the use of FRET in polymers has been pioneered by Morawetz in the 1980s, only recently the technique was extended to obtain quantitative detailed information on nanostructured materials. This review describes a new tool that can be used to analyze FRET in nanostructures and characterize their morphology and component distribution. We describe the application of this tool to a few examples of polymer systems containing nanodomains and heterogeneous distributions of the components, from block copolymer films and micelles to polymer nanoparticles.

Introduction

Nanosized structural elements appear in many polymeric materials, either as a result of their processing (e.g., in polymer blends and particle dispersions) or by design (as in films and micelles obtained by self-assembling of block copolymers). The properties, reliability, and function of composite polymer materials are often dominated by the nanodomains formed at the interfaces between their constituents, which are more susceptible to deformation, fracture, and chemical degradation than the bulk material. Domains with dimensions of a few nanometers can be generated during the synthesis, self-assembling, or melt processing of polymer materials because most polymers do not mix due to the unfavorable balance between the enthalpy and the entropy of mixing. If the materials are quenched to a temperature below the glass transition temperatures of the polymers, nonequilibrium but kinetically stable morphologies develop before the system is able to reach complete phase separation. [1]

The morphological characterization of nanoscale structures is a very active area. Although various microscopy techniques can provide impressive visualization of surface nanodomains, in the majority of cases, this has only resulted in geometric information about the structures. For a more complete characterization of nanodomains, one would like to gain information not only about its size and shape but also on the distribution profile of the various components across the system. If sufficient phase contrast can be established, X-ray and neutron scattering provide two of the most powerful techniques for determining distribution profiles (with resolutions in the Å and nm length-scales respectively). These techniques are sensitive to the sharpness of the interface between components with different contrast factors, but rely in the analysis of deviations from Porod−Law scattering in a region where the scattering intensity is usually very weak. Neutron reflectivity is more rigorous, but limited to systems of lamellar geometry because it analyses the specular reflection between two thin films. Both the reflectivity and the scattering techniques require appropriate corrections of artifacts in the data, such as the waviness at the interface which increases its apparent diffuseness. Additionally, neutron techniques usually involve the synthesis of sample with extensively deuterated areas.

José Paulo S. Farinha, born in Lisbon, Portugal, in 1967, received his Ph.D. from Instituto Superior Técnico (Technical University of Lisbon, Portugal) in 1996, and spent 2 years as a Postdoctoral Fellow with Professor M. A. Winnik at the University of Toronto, Canada. He is currently a Professor of Physical Chemistry, Materials and Nanoscience at IST, in Lisbon. His main research interests are focused on the preparation of polymer nanoparticles and polymers of controlled architecture, and their characterization by photophysical methods.

An alternate approach to study nanodomains in polymer systems is resonance energy transfer. Resonance energy transfer as described by Förster[2,3] was first used to characterize polymer systems, and notably polymer interfaces, by Morawetz.[4] A major advance in the understanding of Förster resonance energy transfer (FRET) in systems with restricted domains was due to Baumann and Fayer[5] and Klafter, Blumen, and collaborators,[6,7] who developed the formalisms to analyze the donor fluorescence

* To whom correspondence should be addressed. E-mail: farinha@ist.utl.pt.

10.1021/jp8016437 CCC: $40.75
Published on Web 07/17/2008

J. M. G. Martinho, born in Portugal, in 1950, received his Ph.D. in Chemical Engineering from Instituto Superior Técnico (Technical University of Lisbon, Portugal) in 1982. In 1985, he joined the Prof. M. A. Winnik research group as a postdoctoral fellow and in 1993 he was invited Professor at the Ontario Center of Materials Research. He is Full Professor of Physical Chemistry and head of the Centro de Química-Física Molecular research center, at IST (Lisbon). His major research interests are in the areas of fast chemical kinetics, photophysics, and polymers.

decay functions in situations where all donor are positioned in equivalent locations and the acceptors are homogeneously distributed in the confined domains. More recently, the theory of FRET has been extended to the case where donors and acceptor occupy nonequivalent positions in restricted domains of planar,[8,9] spherical,[10–12] or cylindrical[13] symmetry, allowing the experimental determination of their concentration profiles in complex nanostructured materials.

In FRET measurements the polymers are labeled with a small amount (typically less than 1 mol %) of a fluorescent energy donor dye (D) and an acceptor dye (A). Upon exciting D with visible or UV radiation, electronic energy can be transferred to a nearby A by a resonance dipole−dipole coupling mechanism. The efficiency of FRET depends on the inverse six power of the distance between D and A in a lengthscale of a few nanometers. This lengthscale matches the size of nanodomains in polymer systems and is small enough to avoid the interference by capillary waves at the interface. In a typical experiment, one mixes two polymer components, one labeled with an energy donor and the other with an acceptor. Phase separation or self-assembling leads to localization of the dyes, either in different domains or at the interface, depending on the sample and the sites chosen for labeling. If separation of D and A labeled domains occurs, a decrease in the quantum efficiency of energy transfer is observed. On the other hand, if both dyes are segregated and colocalized at an interfacial region, one observes an increase in the quantum efficiency of energy transfer. Since the dye distribution mimics the distribution of the polymer components, these experiments can provide detailed information on the distribution of the labeled polymer components and the morphology of the nanostructure.

The widespread application of FRET to biological systems (proteins, membranes, DNA, etc.) is based in similar experimental strategies, but poses different problems. Although in the application of FRET in polymer systems one has to worry about the distribution of an ensemble of dyes (often in restricted domains) with donors and acceptors at different distances, in most biological applications of FRET, it is more usual to have isolated donor−acceptor pairs and assume that the dyes are at fixed distances. In many cases, the models used to analyze FRET in the later systems can be derived from the models that consider nonhomogeneous dye distributions.

Many polymer materials present nanodomains at the interface between different components, from films and micelles obtained by block copolymer self-assembling to polymer blends and polymer nanoparticle dispersions. Here, we will focus on the application of FRET to characterize the distribution of the different components in nanodomains present in copolymer structures and at the surface of polymer nanoparticles.

In block copolymers, different polymers are attached at a common junction, so that the degree of phase separation is limited by the covalent bond between the blocks. For this reason, block copolymers self-assemble to form equilibrium structures that depend on the balance between the unfavorable energy of mixing and the entropy penalty for localization of the block junctions. The periodic uniformly sized and shaped nanostructures formed in films of block copolymers over macroscopic distances have been used as a template to create patterns for the preparation of functional nanostructures and nanodevices,[14] such as photonic materials, fuel cells, batteries, optoelectronic devices, bioactive surfaces for diagnostic chips, and implant surfaces to control cell adhesion. Block copolymers are also a promising platform for the direct fabrication of three-dimensional structures for high-density information storage media and sub-22 nm lithography.[15] When assembled into micelles, block copolymers can be used as surface modification agents, nanoreactors, small-molecule delivery vehicles, in lithography, to create nanoparticle arrays, etc.

The process of block copolymer self-assembling into phase separated nanostructures is primarily determined by the overall degree of polymerization N, the magnitude of the Flory−Huggins interaction parameter χ of the polymers, and the volume fractions of the blocks.[16] Above $\chi N \approx 10$, block copolymers form self-assembled nanostructures, with interfacial domains between the blocks that are usually a few nanometers thick. Periodic lamellar structures are formed for blocks of approximately the same length, with hexagonal cylindrical and body centered cubic spherical morphologies appearing for increasingly asymmetric blocks. More complex bicontinuous morphologies are formed for boundary compositions between lamellar and cylindrical structures.[17,18] Block copolymers also self-assemble in solvents selective for one of the blocks to form micelles with a core of insoluble block surrounded by a corona of solvent-swollen soluble block, in a wide range of morphologies.[19] In this case, the thickness of the interfacial domains between blocks also depends on the solvent.[20] The swelling of the (soluble) corona polymer by the solvent leads to the decrease of the core−corona interface thickness because the (insoluble) core segments try to avoid contact with the solvent.[21]

Nanodomains also play an important role in polymer nanoparticles. Many polymers of industrial importance are prepared as water dispersions of spherical particles with diameters of ca. 100 nm to a few microns. These particles are used in a variety of applications, from paints and inks to high impact resistant polymers and specialty coatings, supports for biomolecules, vectors for drug delivery, bioseparation, etc.[22] Since the large surface area of polymer nanoparticles play a central role in most of their applications, it is important to know the morphology of the polymer−water interfacial domains. These are usually a few nanometers thick, depending on the surface charge density resulting from the synthetic procedure used to prepare the particles, the ionic strength of the aqueous medium and the characteristics of the polymer segments at the interface.[23]

In the following sections, we will describe the FRET models necessary to determine the distribution of donor and acceptor dyes in systems with restricted dimensions, and we give

examples of their application to characterize the component distribution and the morphology of nanodomains in block copolymer structures and polymer nanoparticles.

Resonance Energy Transfer in Nanodomains

Sixty years ago, Förster showed that the rate of resonance energy transfer from an electronically excited donor (D*) to an acceptor (A) separated by a distance r is given by[2,3]

$$w(r) = \frac{1}{\tau_D}(R_0/r)^6 \quad (1)$$

where τ_D is the donor lifetime in the absence of acceptors and R_0 is the critical Förster radius (the distance for which energy transfer equals the natural deactivation of D*). The value of R_0 sets the lengthscale of FRET for a given pair of dyes and depend on their spectroscopic properties

$$R_0^6 = \frac{9000(\ln 10)\kappa^2\varphi_f}{128\pi^5 N_A n^4}\int_0^\infty F_D(\lambda)\varepsilon_A(\lambda)\lambda^4\,d\lambda \quad (2)$$

In eq 2, the integral accounts for the spectral overlap of the normalized donor fluorescence spectrum $F_D(\lambda)$, with the absorption spectrum of the acceptor $\varepsilon_A(\lambda)$ ($M^{-1}cm^{-1}$). The Förster radius also depends on the donor fluorescence quantum yield ϕ_f in the absence of acceptor, the refractive index n of the medium in the wavelength range of spectral overlap, and the orientation factor κ^2, which depends on the angle between the transition dipole moments of the D and A molecules θ_{DA}, and the angles θ_D and θ_A between each of these dipoles and the vector connecting their centers

$$\kappa^2 = (\cos\theta_{DA} - 3\cos\theta_D\cos\theta_A)^2 \quad (3)$$

For a single D−A pair, the value of κ^2 is in the range of 0 to 4 but for an ensemble of D−A pairs, κ^2 is usually preaveraged over the distribution of all orientations to give $\langle\kappa^2\rangle = 2/3$ if the molecules undergo rotational motion faster than the fluorescence lifetime, and $\langle\kappa^2\rangle = 0.476$ if the dipoles are randomly oriented and do not rotate on the time scale of fluorescence.[24,25] When none of these limits apply, it is more difficult to obtain information on the donor−acceptor separation distance.[26] If the rotation dynamics of the dyes is of the order of the time scale for energy transfer, information on the separation distances can be obtained from time-resolved depolarization measurements.[27,28] On the other hand, if the dyes are immobile and have nonisothropic orientations, as for example in the case of donor and acceptor dyes in DNA stands, it is possible to measure the variation of the orientation parameter with the relative position of the dyes.[29] However, in most situations the dyes are not strictly immobile during the time-scale of FRET, and their rotational mobility is usually sufficient to allow the use of $\langle\kappa^2\rangle = 2/3$ within an error of less than ca. 10%.[30] This is specially the case when the analysis of time-resolved depolarization of the dyes yields mobilities corresponding to a wobbling movement in a cone with internal angle above 30°.[31]

Resonance energy transfer does not depend on the properties of the donor−acceptor pair alone, but also on the geometry and dynamics of the system, which affect the distance between donor and acceptor. Many systems of interest have a distribution of D−A distances, either arising from the confinement of the dyes in a restricted space, and/or from heterogeneous distributions of D and A in the structure. In order to use FRET to characterize nanodomains in polymer systems, the experimental data should be analyzed taking into account both the restricted dimensions of the domains and the distribution of the different components. Here, "restricted dimensions" refer to a space or domain confining the dyes in which at least one dimension is on the order of the lengthscale of FRET (i.e., a few nanometers).

In systems characterized by a distribution of D−A distances, the donor fluorescence decay corresponds to a distribution of decay times associated with the transfer between pairs at different distances, because of the r^{-6} dependence of the rate of resonance energy transfer. While for isolated excited donors surrounded by acceptors at a constant distance r the survival probability is still exponential (but faster than for the unquenched donor), for a homogeneous distribution of D and A in an infinite media the donor decay function is a stretched exponential, because the donors are surrounded by acceptors at different distances[32]

$$I_D(t) = \exp\left(-\frac{t}{\tau_D}\right)\exp\left[-P\left(\frac{t}{\tau_D}\right)^\beta\right] \quad (4)$$

Here, $d = 6\beta$ is the dimensionality of the media (which is equal to the Hausdorff dimension if the dyes are embedded in a fractal lattice) and P is related to the local number of acceptors c_Δ in a Δ-dimensional sphere of radius R_0 (Γ is the Gamma function)

$$P = c_\Delta\left(\frac{3\kappa^2}{2}\right)^\beta\Gamma(1-\beta) \quad (5)$$

El-Sayed and co-workers[21] were the first to report the utility of eq 4 as a phenomenological expression to analyze FRET in systems of restricted geometry. In this case, an apparent fractional dimension is sometimes obtained due to edge effects of the confining space. Although the application of eq 4 to systems of restricted geometry is strictly empirical, the apparent dimension parameter can give some information on the nature of the domains where D and A are distributed. [33]

Effect of Restricted Geometry: Donors in Equivalent Locations. The first attempt to rigorously describe resonance energy transfer in a system of restricted geometry was done by Fayer and co-workers for D-D homotransfer (energy migration),[34] and by Klafter, Blumen, and co-workers for FRET[35]

$$I_D(t) = \exp\left(-\frac{t}{\tau_D}\right)\phi(t) \quad (6)$$

$$\phi(t) = \exp\left(-p\int_V\{1-\exp[-w(r)t]\}\rho(r)\,dV\right) \quad (7)$$

where $\varphi(t)$ is the donor survival probability with respect to FRET, V is the volume of the restricted space where the donors and acceptors are distributed, $w(r)$ is the rate of energy transfer defined in eq 1, $\rho(r)$ is the probability distribution of finding an acceptor at a distance r from the donor, and p is the probability of occupation by the acceptors, which measures the acceptor concentration. This expression was integrated for a number of simple structures,[8,9] but since eqs 6 and 7 can only be used for systems in which all the donors occupy equivalent positions, they have limited applicability in real nanostructured systems.

More recently, new tools were developed to obtain the survival probabilities whenever D and A concentration profiles follow an element of planar,[10–12] spherical,[13] or cylindrical[8] symmetry. This theoretical methodology overcame the restriction of equivalent donor positions, and so opened the doors for handling more complex nanostructures.

Arbitrary Distributions of Donor and Acceptor Dyes. In order to calculate the donor fluorescence survival probability in systems with arbitrary distribution functions of D and A dyes, it is necessary to account for the difference in the distribution of A surrounding D dyes in different locations. This required

the development of new analysis tools, known as distribution models for energy transfer.

Energy transfer models that take into account the distribution of D and A in restricted geometry were first derived for systems with planar concentration gradients arising from D and A labeled polymer chains diffusing across an interface,[9] and then used to describe simple planar systems with restricted dimensions and homogeneous distributions of D and A.[10] An equivalent model for spherical-symmetric systems was also developed and used to analyze experimental results of diffusion in films obtained from polymer colloids,[12] and to model FRET in simple spherical systems of restricted geometry[11] and in block copolymer films.[13] A model for cylindrical geometry was only developed later, due to its higher mathematical complexity.[10]

The basis of the models that describe FRET is the survival probability of a donor at a position $\mathbf{r}_D$ in the presence of an acceptor at position $\mathbf{r}_i$

$$f(t, \mathbf{r}_D, \mathbf{r}_i) = \exp[-t\omega(|\mathbf{r}_i - \mathbf{r}_D|)] \tag{8}$$

If we consider that donors and acceptors occupy discrete sites in a restricted space and assume that the acceptors act independently, the donor survival probability φ is given by the product of eq 8 weighted by the distribution function, $g(\mathbf{r}_i, j)$, of the number of acceptors j, in each site $\mathbf{r}_i$

$$\phi(t, \mathbf{r}_D) = \prod_{\mathbf{r}_i \neq \mathbf{r}_D} \left\{ \sum_j g(\mathbf{r}_i, j)[f(t, \mathbf{r}_D, \mathbf{r}_i)]^j \right\} \tag{9}$$

If the probability of having one acceptor at $\mathbf{r}_i$ is small, the probability that j acceptors exist at the site $\mathbf{r}_i$ is given by a Poisson distribution with mean equal to the number of acceptors $n_A(\mathbf{r}_i)$

$$g(\mathbf{r}_i j) = \exp[-n_A(\mathbf{r}_i)] \frac{n_A^j(\mathbf{r}_i)}{j!} \tag{10}$$

and, considering that the donor is inside a continuous restricted space of volume V, the donor decay probability rearranges to

$$\phi(t, \mathbf{r}_D) = \exp\left(-\int_V C_A(\mathbf{r}_A)\{1 - \exp[-t\omega(|\mathbf{r}_A - \mathbf{r}_D|)]\}\, d\mathbf{r}_A\right) \tag{11}$$

The integral in eq 11 is performed over the volume elements $d\mathbf{r}_A$ containing acceptors with number density $C_A(\mathbf{r}_A)$. The function $\varphi(t,\mathbf{r}_D)$ measures the probability that an excited donor, located at $\mathbf{r}_D$ "survives" for a time t before losing its excitation by energy transfer. Donors located at different positions are surrounded by different acceptor distributions and so the donor decay has to be averaged over all the donors in the system

$$I_D(t) = \exp\{-t/\tau_D\} \int_V C_D(\mathbf{r}_D)\, \phi(t, \mathbf{r}_D)\, d\mathbf{r}_D \tag{12}$$

where $C_D(\mathbf{r}_D)$ is the concentration profile of D.

The last two equations describe the donor decay probability when FRET occurs between donors and acceptors distributed in a confined space. The geometric restrictions are introduced by the volume V, and the heterogeneity of D and A distributions by position-dependent donor and acceptor concentration profiles. This general formalism can be simplified when the donor and acceptor distributions have spherical, planar or cylindrical symmetry.

Spherical Symmetry. We now consider the particular case of spherical symmetric distribution functions of donor and acceptor dyes. In this case, the survival probability of a donor located at $\mathbf{r}_D$ (eq 11) can be integrated in spherical coordinates[36]

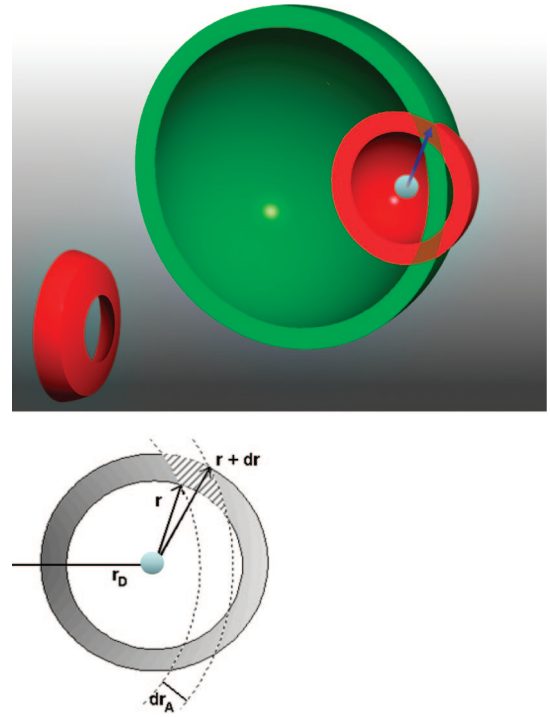

Figure 1. The interception of the donor-centered energy transfer rate function $w(r)$ (top, slice with constant donor−acceptor distance shown in red) with a spherical acceptor concentration profile (top, slice with constant acceptor concentration shown in green) originates a ring shaped volume element where the two functions are constant (shown middle left) with a cross section as represented bellow, and volume given by eq 15.

$$\phi(t, \mathbf{r}_D) = \exp\left(-\int_{-\pi}^{\pi}\int_0^{\pi}\int_{R_e}^{\infty} C_A(r_A)\{1 - \exp[-\omega(r)t]\} r^2 \sin\varphi\, dr\, d\varphi\, d\theta\right) \tag{13}$$

where R_e is the donor−acceptor encounter distance (their minimum approach distance), usually taken to be the sum of the donor and acceptor van der Waals radii.[10] The acceptor radial position r_A is given by the sum of the vectors defining the donor position $\mathbf{r}_D$ and the D−A distance $\mathbf{r}$

$$r_A = |\mathbf{r}_D + \mathbf{r}| = \sqrt{r^2 + r_D^2 + 2\mathbf{r}\mathbf{r}_D \sin\varphi \cos\theta} \tag{14}$$

The integration of eq 13 can be simplified by noticing that the acceptor concentration profile $C_A(r_A)$ is symmetric relative to the origin, while the rate of energy transfer $\omega(r)$, which depends on the D−A distance, is symmetric relative to the donor position. [12] The product $C_A(r_A)\{1 - \exp[-\omega(r)\, t]\}$ is therefore invariant in the volume element defined by the interception of one spherical shell centered at the origin with radius r_A and width dr_A, and another centered in the donor position $\mathbf{r}_D$ with radius r and width dr (Figure 1). This defines a volume element dv that resembles a concave ring

$$dv = 2\pi \frac{r r_A}{r_D}\, dr\, dr_A \tag{15}$$

The integral is calculated over all rings, from $r_D - r$ to $r_D + r$, for each D−A separation r to give the average concentration of acceptors over each ring. Finally, integration over all D−A distances yields

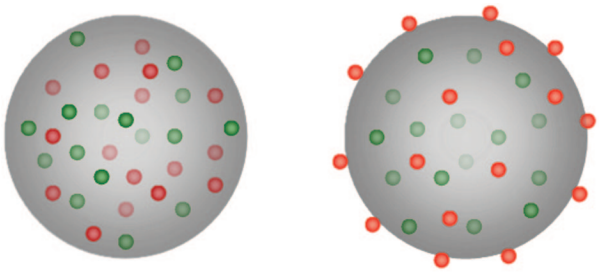

Figure 2. Simple cases that cannot be treated with eqs 6 and 7 because the donors are in nonequivalent positions: donors (green) and acceptors (red) uniformly distributed inside a sphere of radius R_s (left); and acceptors in the surface of a sphere with donors inside (right).

$$\phi(t, \mathbf{r}_D) = \exp\left(-\frac{2\pi}{r_D}\int_{R_e}^{\infty}\{1-\exp[-\omega(r)t]\}\left[\int_{r_D-r}^{r_D+r} C_A(r_A) r_A \, dr_A\right] r \, dr\right) \quad (16)$$

With eqs 12 and 16, it is possible to calculate the donor fluorescence decay curve in systems with any donor and acceptor concentration profiles that have spherical symmetry.

These expressions can also be used to obtain the donor decay curve for a number of simple situations in which the donors are in nonequivalent positions,[21] that could not be treated with eq 4. A particularly simple application of the model allows the calculation of the radius of a spherical particle containing D and A dyes in the surface. This was used to obtain the core radius in micelles of block copolymer labeled in the junction between blocks.[8]

When the acceptors are distributed in the surface of a sphere of radius R_s and the donors are inside (Figure 2), the donor and acceptor density profiles are given by $C_D(r_D) = C_D H(R_s - r_D)$ for $0 \le r_D \le R_s$ and $C_A(r_A) = C_{A0}\,\delta(R_s - r_A)$, where H and δ are the Heaviside and the delta functions and C_{D0} and C_{A0} are the number density of donors and acceptors, respectively. In this case, the integral in r_A of eq 16 has a nonzero value only if the peak of the delta function lies in the domain of integration. Therefore, the conditions $|r_D - r| < R_s$ and $r_D + r > R_s$ should be simultaneously satisfied ($R_s - r_D \le r \le R_s + r_D$) leading to

$$I_D(t) = \exp(-t/\tau_D)\int_o^{R_s} \phi(r_D, t) 4\pi r_D^{\,2} \, dr_D \quad (17)$$

$$\phi(r_D, t) = \exp\left(-\frac{2\pi n_A R_s}{r_D}\int_{R_s-r_D}^{R_s+r_D}\{1-\exp[-w(r)t]\} r \, dr\right) \quad (18)$$

Another interesting and useful case, is when both donors and acceptors are uniformly distributed inside a sphere (Figure 2). In this case, $C_D(r_D) = C_{D0}\,H(R_s - r_D)$ with $0 \le r_D \le R_s$ and $C_A(r_A) = C_{A0}\,H(R_s - r_A)$ with $0 \le r_A \le R_s$, yielding

$$\phi(r_D, t) = \exp\left(-4\pi n_A\int_0^{R_s-r_D}\{1-\exp[w(r)t]\} r^2 \, dr - \frac{\pi n_A}{r_D}\int_{R_s-r_D}^{R_s+r_D}\{1-\exp[w(r)t]\}[R_s^{\,2}-(r_D-r)^2] r \, dr\right) \quad (19)$$

Planar Symmetry. In a system with a plan of symmetry, the donor and acceptor concentrations change only along an axis z. The donors in each slice perpendicular to the z axis are surrounded by different acceptor concentrations. Consequently, the donor decay can be evaluated as a sum over all slices

$$I_D(t) = \exp(-t/\tau_D)\int_V C_D(z)\phi(t, z) \, dz \quad (20)$$

The donor survival probability for a slice positioned at z, $\varphi(t,z)$, depends on the acceptor concentration around it[8,9]

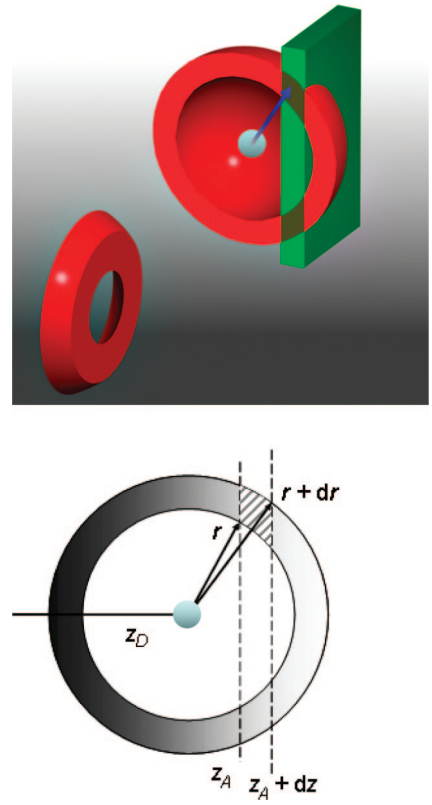

Figure 3. The interception of $w(r)$ (top, slice with constant donor−acceptor distance shown in red) with a lamellar acceptor concentration profile (top, vertical cut with constant acceptor concentration shown in green) originates a ring shaped volume element (shown middle left), with a cross section as represented bellow and volume given by eq 22.

$$\phi(t, z) = \exp\left(-\int_0^{2\pi}\int_0^{\pi}\int_{R_e}^{\infty} C_A(z_A)\{1-\exp[-\omega(r)t]\} r^2 \sin\varphi \, dr \, d\varphi \, d\theta\right) \quad (21)$$

where z_A is the distance from a given acceptor to the plane at $z = 0$ perpendicular to the z axis. Again, this equation can be simplified because the distribution function of acceptors is uniform in any thin vertical slice of a spherical shell centered on the donor position (Figure 3).[8] The volume of the ring defined by the intersection of the spherical shell of radius r and width dr, with a slice of width dz perpendicular to the z axis is

$$dv = 2\pi r \, dr \, dz \quad (22)$$

Following a procedure identical to that used for spherical symmetry, one obtains[37]

$$\phi(t, z) = \exp\left(-2\pi\int_{R_e}^{\infty}\{1-\exp[-\omega(r)t]\}\left[\int_{z-r}^{z+r} C_A(z_A) z_A \, dz_A\right] r \, dr\right) \quad (23)$$

Equations 20 and 23 can be used to calculate the fluorescence donor decay curve for systems with a plan of symmetry where the donor and acceptor concentration can have any kind of distribution profiles.[8,11,38,39]

Using eqs 20 and 23, it is possible to obtain the donor decay curve for a number of simple systems of interest, not only in polymers but also in the biological sciences. For example, most FRET measurements in model biological membranes have been analyzed using equations for FRET in planar systems. From eqs 20 and 23, it is possible to obtain the expression for FRET

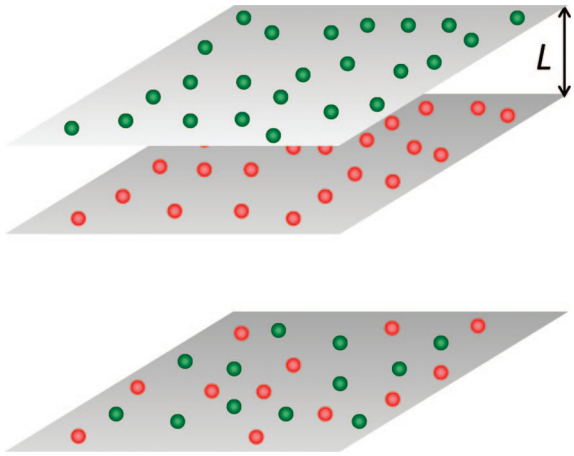

Figure 4. Planar systems used to model FRET in biological membranes: donors (green) and acceptors (red) uniformly distributed in parallel planes separated by a distance L (top); and coplanar donors and acceptors (bottom).

in systems with coplanar donors and acceptors (Figure 4 bottom), first derived by Hauser et al.,[40] subsequently extended by Wolber and Hudson,[41] and presented in an approximate form by Dewey and Hammes.[42] Since donors and acceptors are located in an infinite plan at $z = 0$, the parametric integral in eq 23 equals C_A and integration in r followed by substitution in eq 20 readily yields

$$I_D(t) = \exp\left[-\frac{t}{\tau_D} - \pi C_A R_0^6 \Gamma\left(\frac{2}{3}\right)\left(\frac{t}{\tau_D}\right)^{1/3}\right] \quad (24)$$

In other systems, the donors and acceptors are located in parallel planes separated by a distance L (Figure 4 top). In this case, the donor survival probability curve was first derived analytically by Fayer[5] and can easily be obtained from eqs 20 and 23 in the form[12]

$$I_D(t) = \exp\left\{-\frac{t}{\tau_D} - \pi C_A R_0^6 \Gamma\left(\frac{2}{3}\right)\left(\frac{t}{\tau_D}\right)^{1/3}[1 - \alpha^{-(1/3)}(1 - e^{-\alpha}) - \Gamma(\tfrac{2}{3}, \alpha)]\right\} \quad (25)$$

$$\alpha = \frac{t}{\tau_D}\left(\frac{R_0}{L}\right)^6$$

$$\Gamma\left(\frac{2}{3}, \alpha\right) = \int_\alpha^\infty x^{1/3} e^x \, dx$$

which is more adequate for fitting experimental time-resolved fluorescence measurements than the approximation proposed by Dewey and Hammes.[43]

Cylindrical Symmetry. Over the past decade there has been an increasing interest in cylindrical structures, such as nanotubes and nanowires, to be used as templates in connection with nanotechnology.[13] Due to its sensitivity in the nanoscale, FRET can be advantageously used to characterize the morphology and composition of these nanostructures. In the past, the use of FRET in cylindrical structures has not gone beyond a qualitative approach because of difficulties in developing a detailed model similar to those obtained for spherical and planar symmetric systems. In fact, the intersection of spherical shells (representing acceptors at fixed distances from a given donor) with cylindrical surfaces (describing regions of constant dye concentration), are given by complex formulas involving elliptic integrals. Only recently was a general expression for FRET in cylindrical systems obtained,[13] by considering an equation similar to eq 13 and the distance between donors located on the surface of a cylinder of radius R_D, and acceptors on a concentric cylindrical shell, of radius R_A and thickness dR_A (Figure 5)

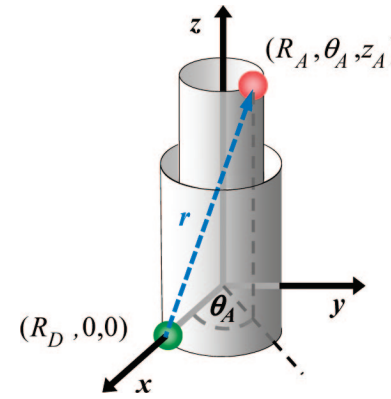

Figure 5. Energy transfer from an excited donor at a distance R_D from the z axis of the cylindrical structure, to an acceptor at a distance R_A from z.

$$r = (R_D^2 + R_A^2 + z_A^2 - 2R_A R_D \cos\theta_A)^{1/2} \quad (26)$$

The energy transfer probability $\varphi(t, R_D)$ for the donor is then

$$\varphi(t, R_D) = 4\exp\left(-\int_0^\infty dz_A \int_0^\infty R_A C_A(R_A)\, dR_A \int_0^\pi \{1 - \exp[-w(r)t]\}\, d\theta_A\right) \quad (27)$$

where the integration is carried out with the volume element $R_A\, dR_A\, d\theta\, dz$ and $C_A(R_A)$ is the acceptor number density at the cylinder of radius R_A.

The donor survival probability in a cylindrical object of total length L is obtained by integration over all possible donor positions

$$I_D(t) = 2\pi L \exp\left(-\frac{t}{\tau_D}\right)\int_0^\infty R_D C_D(R_D)\phi(t, R_D)\, dR_D \quad (28)$$

where $C_D(R_D)$ is the donor concentration profile. Using eqs 26–28, it is possible to calculate the donor fluorescence decay profile for virtually any distribution of D and A obeying cylindrical symmetry.[44] In systems with restricted geometry or finite size, $C_A(R_A)$ and $C_D(R_D)$ have to be associated with appropriate truncating functions that restrict the domain of integration. The minimum D−A approach distance can be introduced analytically or numerically, by excluding values $r < R_e$ in the integration.

Data Analysis

In systems where the donor can only transfer to a single acceptor at a fixed distance, as in the folding of labeled proteins or in the detection of labeled RNA, the donor−acceptor distance can be obtained from the quantum yield of energy transfer (Φ_{ET}). This can be obtained from steady state measurements of the fluorescence intensity of the donor in the presence (F_D) and absence (F^0_D) of the acceptor

$$\Phi_{ET} = 1 - \frac{F_D}{F_D^0} \quad (29)$$

To avoid experimental problems in the determination of F_D and F^0_D, such as the common distortion of the donor spectra by inner filter effects, light scattering or residual acceptor emission, it is more convenient to calculate Φ_{ET} from the

fluorescence decay of the donor in the presence (I_D) and absence (I^0_D) of the acceptor

$$\Phi_{ET} = 1 - \frac{\int_t I_D(t)\,dt}{\int_t I^0_D(t)\,dt} \tag{30}$$

However, in systems where transfer to several acceptors at different distances from the donors is possible, and detailed information on the distribution of the donors and acceptors is mandatory, it is necessary to analyze the shape of the donor fluorescence decay curve.

Generally, it is possible to obtain the decay parameters by fitting the donor fluorescence decay curves using a nonlinear algorithm.[45,46] However, for complex systems, notably when donors and acceptors are heterogeneously distributed in domains of restricted geometry, it is advisable to use a grid mapping technique. One first simulates a series of donor fluorescence survival probability curves, calculated using the appropriate equation for $I_D(t)$ (according to symmetry of the system), and a parametrized equation of the donor and acceptor concentration profiles. Usually the orientation parameter $\langle\kappa^2\rangle$, the critical Förster radius R_0, and the donor intrinsic lifetime τ_D, can be fixed to values obtained from independent experiments, and so it is only necessary to change the parameters of the equations describing the donor and acceptor distributions. The simulated donor fluorescence survival probability curves are then convoluted with the experimental instrument response functions $L(t)$[46]

$$I^{conv}_D(t) = \int_0^t L(s) I_D(t-s)\,ds \tag{31}$$

and finally, the experimental decay profiles $I^{exp}_D(t)$ are fitted to each of the simulated $I^{conv}_D(t)$ curves, using a linear convolution algorithm where the only fitting parameter is the normalization factor of the decay intensity a_N

$$I^{exp}_D(t) = a_N I^{conv}_D(t) \tag{32}$$

The quality of the fitting results is evaluated from the plot of the reduced χ^2 as a function of the distribution parameters. After identifying the minima on the plots, the weighted residuals and the autocorrelation of residuals are compared to obtain the best fit.[46]

Block Copolymer Nanostructures

In spite of the strong interest in block copolymer structures, there are very few data on the nanodomains that constitute the interfacial region between different blocks. Fredrickson was probably the first to recognize the utility of FRET to study block copolymers.[47,48] In order to characterize the interface between blocks, two identical copolymers are labeled at the block junction, one with a fluorescent donor dye (D) and another with an acceptor dye (A). Mixing of the two copolymers and subsequent self-assembling leads to confinement of the dyes at the interface (Figure 6), with an increase in FRET efficiency.

In early experiments, fluorescence decay curves obtained for junction-labeled block copolymers have been analyzed using eq 4, to obtain qualitative information on the interface. In order to effectively characterize the morphology and density profile of the interfacial domain between the blocks, it is necessary to use a model that describes the kinetics of FRET in restricted geometry with nonhomogeneous donor and acceptor distributions. In the case of junction labeled block copolymer films with a periodic lamellar structure, one can use eqs 20–23, coupled to a model that describes the shape of the D and A concentration profiles (which in turn are related to the local morphology of the film). The shape of the interfacial domains between blocks is given by the junction distribution function $g_J(z)$, which can be calculated by the model of Helfand and Tagami for equilibrium phase-separated block copolymers in the strong segregation regime[47,48]

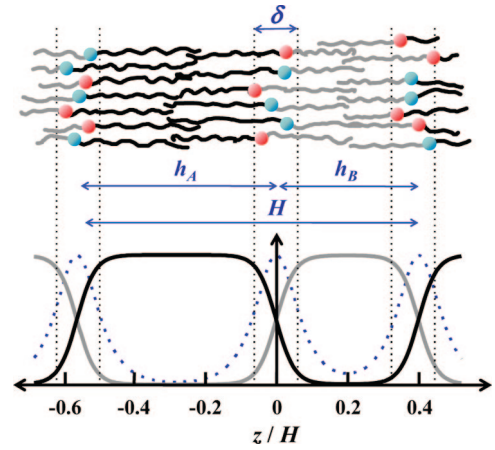

Figure 6. Phase separated diblock copolymer originating a lamellar morphology. The copolymer is labeled at the junction between blocks with either a donor (○) or an acceptor (●). The polymer volume fraction profiles originate a periodic junction distribution function (•••) that can be calculated with the Helfand−Tagami model, eq 33 (shown here for an interface thickness $\delta = H/10$, with $H = h_A + h_B$).

$$g_J(z) = \frac{(2/\pi)}{\delta}\,\mathrm{sech}(2z/\delta) \tag{33}$$

The interface thickness δ, measured along a direction z perpendicular to the interface, can in turn be expressed in terms of the Flory−Huggins χ interaction parameter and the statistical segment length b, averaged for the polymers of the two blocks[49]

$$\delta = \frac{2b}{\sqrt{6\chi}} \tag{34}$$

This method has been tested with respect to its sensitivity toward the D/A distribution shape,[25,50] the influence of the dipole orientation factor in block copolymer films,[38] and the relation with the apparent dimension obtained with eq 4.[38,39,49,51–53] Unlike neutron reflectivity, which cannot distinguish between the diffuseness and waviness of the interface, FRET can be used to determine the interface thickness with no capillary wave correction. FRET has been used to determine the interface thickness in a variety of block copolymer films.[54,55] The results compare well with interface thickness values of 5.1 and 7.7 nm obtained by neutron reflectivity in thin films of poly(styrene-*b*-methyl methacrylate)[56] and poly(styrene-*b*-butyl methacrylate),[57,58] respectively, as well as with the interface thickness of 1.8 nm obtained by SAXS for poly(isoprene-*b*-styrene) films.[21]

In block copolymer micelles, the interface geometry is further influenced by the solvent swelling the micelle corona. In a poor solvent for the core-block, there is no swelling of the core, and so the solvent only influences the width of the interface. If we consider the case of spherical micelles of junction labeled block copolymers, the shape of the radial dye distribution (Figure 7, top) can be described by modifying eq 33, in order to account for the curvature of the micelle interface[20,21]

$$g_J(r) = \frac{1}{n_J \cosh[2(r - R_s)/\delta]} \tag{35}$$

where δ is the interface width (Figure 7), R_s is the radius of the

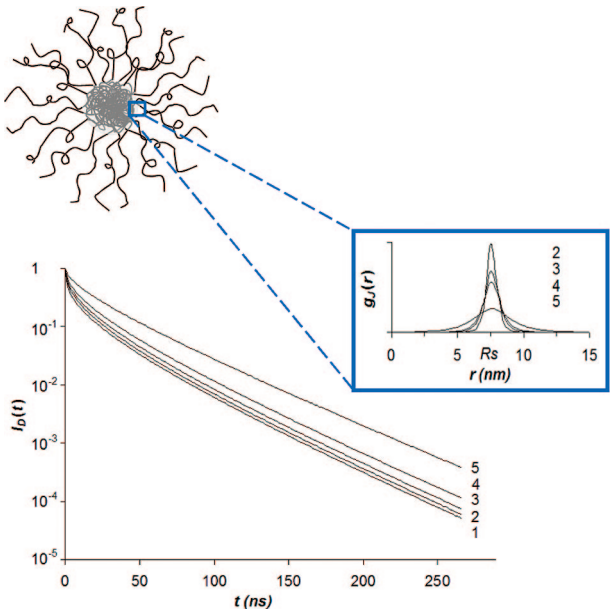

Figure 7. Probability $g_J(r)$ of finding the block junction points at a distance r from the center of the micelle (inset), for a distribution of block junction points given by eq 35 for different interface thickness values: 0 nm (**1**), 0.6 nm (**2**), 0.9 nm (**3**), 1.2 nm (**4**), and 2.4 nm (**5**). The corresponding donor fluorescence decay functions (bottom) were simulated using eqs 12 and 16 for micelles with core radius $R_s = 7.6$ nm, $\langle\kappa^2\rangle = 2/3$, $R_0 = 2.3$ nm, $\tau_D = 45.5$ ns, and $R_e = 0.5$ nm.

micelle core, and n_J is a normalization constant

$$n_J = 4\pi \int_0^\infty \frac{r^2}{\cosh[2(r - R_s)/\delta]}\, dr \qquad (36)$$

Experimental donor fluorescence decay curves can be analyzed using eqs 35 and 36 to describe the shape of the junction point distribution and eqs 12 and 16 to model the FRET kinetics in the restricted geometry of the interface region. Simulated donor fluorescence decay curves (Figure 7,bottom) show that when the interface thickness increases, the donor fluorescence decay becomes significantly slower because the dye concentration in the interface decreases, increasing the D−A separation and thus decreasing the overall energy transfer efficiency.

Results obtained for mixtures of phenanthrene and anthracene labeled polyisoprene-*b*-poly(methyl methacrylate) (PI-PMMA) diblock copolymers in acetonitrile (a poor solvent for PI) show that the copolymers self-assemble into star-like micelles with a dense core of insoluble PI blocks and a soft solvent-swollen PMMA corona.[21] The thickness of the interfacial domain between the core and the corona was obtained by comparing the experimental donor fluorescence decay curves with simulated curves (using $\langle\kappa^2\rangle = 2/3$ because the PI block is in the molten state a room temperature), to yield $\delta = 0.9 \pm 0.1$ nm (Figure 8).[23,59]

Polymer Nanoparticles

Although polymer nanoparticles dispersed in water are usually seen as glassy or rubbery spheres with a sharp surface, there is evidence of a "hairy" polymer shell at the particle/water interface (Figure 9).[32,60] Many properties of polymer nanoparticles depend on this interfacial domain, which conditions the availability of surface chemical groups and charges. FRET has been used to measure this fuzzy interfacial domain by adsorbing energy donor and acceptor dyes onto the particle surface. Analysis of the donor fluorescence decays with eq 4 has yielded apparent fractal

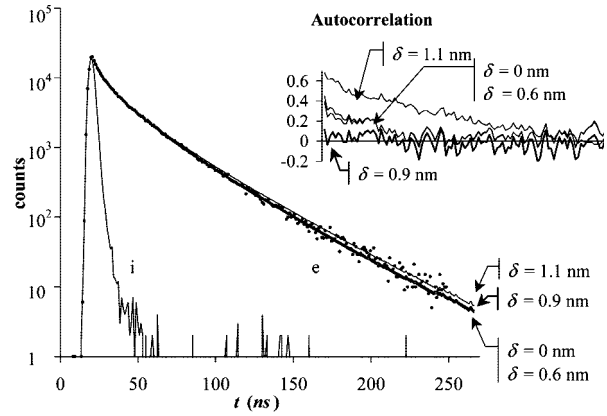

Figure 8. Experimental instrument response function (i) and donor decay profile of labeled PI-PMMA block copolymer micelles in acetonitrile (e), fitted with decay curves simulated for different interface thickness values. The autocorrelation of the weighted residuals is only homogeneous for $\delta = 0.9$ nm.

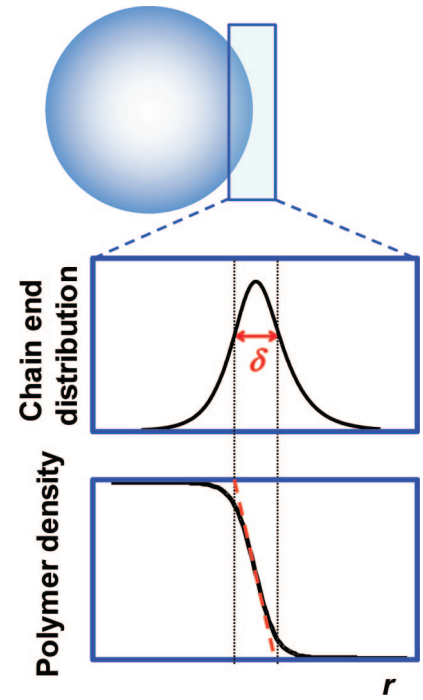

Figure 9. Cartoon of a polymer nanoparticle with a distribution of polymer chains at the polymer−water interface. The density profile of polymer chain ends at the interface is described by eq 35 (middle). The thickness of the interface δ is defined from the intercepts of the tangent line at the inflection point of the polymer density profile (bottom).

dimensions around $d \approx 2$, characteristic of a random distribution of dyes on a flat surface,[61] and sometimes lower ($d \approx 1.8$) due to limitations of the model.[23] However, detailed information on the characteristics of the interfacial domains can be obtained using eqs 12 and 16 to describe the FRET kinetics and eq 35 for the shape of the polymer density profile (Figure 9).[23]

Analysis of the donor fluorescence decay curves of water dispersions of polystyrene particles (PS, 100 nm diameter) containing adsorbed rhodamine 6G (R6G) as the energy transfer donor and malachite green (MG) as the acceptor, yielded interface thickness values of $\delta = 2.0 \pm 0.1$ nm and $\delta = 2.9 \pm 0.2$ nm, that correlate very well with the particle surface charge densities of 1.7 μC m^{-2} and 2.3 μC m^{-2}, respectively (Figure 10). The increase in the interface domain thickness is mainly due to the electrostatic repulsion between the negatively charged

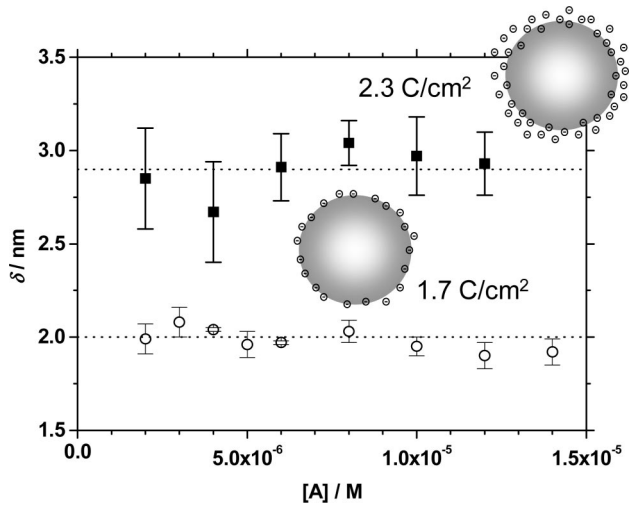

Figure 10. Variation of the interface thickness δ (Figure 9) with the bulk acceptor concentration, obtained by fitting the donor fluorescence decay curves for particles with surface charge densities of 1.7 μC m^{-2} (○) and 2.3 μC m^{-2} (■).

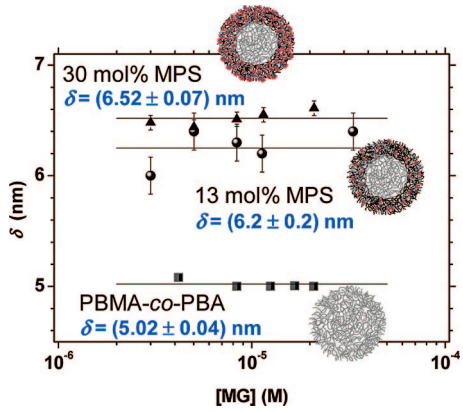

Figure 11. Schematic view of the cross-linked core−shell poly(butylmethacrylate-*co*-butylacrylate) nanoparticles with a low T_g core and a TMS-functionalized shell. Interface thickness obtained by FRET analysis for different bulk acceptor concentration without TMS (■) and with 13 mol % (●) and 30 mol % (▲) TMS in the shell.

polymer chain ends resulting from the initiator used in the emulsion polymerization.[62–64]

In another set of experiments, monodispersed poly(butylmethacrylate-*co*-butylacrylate) cross-linked core−shell nanoparticles (ca. 100 nm diameter) were functionalized with trimethoxisilane (TMS) groups in the outer shell. The TMS groups covalently bind the rubbery particles to a nanostructured silica network, in the controlled sol−gel synthesis of highly porous, hydrophobic, inorganic−organic nanostructured aerogels. [65] Fluorescence decay measurements performed in situ on water dispersions of these nanoparticles containing a pair of adsorbed cationic dyes (R6G and MG) were analyzed with a distribution model for FRET, to obtain the distribution of the dyes at the nanoparticle/water interface.[62–64] The nanoparticle−water interface thickness of the particles without TMS groups (Figure 11), $\delta = (5.02 \pm 0.04)$ nm, is higher than for the PS particles (Figure 10) as expected from the higher glass transition temperature of PS. For particles with a TMS-functionalized shell, the interface is even broader as a result of the increase in free volume caused by the bulky TMS groups: $\delta = (6.2 \pm 0.2)$ nm and $\delta = (6.52 \pm 0.07)$ nm for particles with 13 mol % and 30 mol % of TMS in the shell, respectively (Figure 11). The minor difference in interface breadth between particles containing different amounts of TMS is due to the increase in diameter caused by the increase in TMS content. The increase in interface thickness, caused by the TMS groups gives a better shell permeability, which enhances the availability of the TMS groups during the formation of the silica network in the sol−gel synthesis of hybrid aerogel materials.[8,9]

Conclusions

Interfacial domains play an important role in different nanostructured polymer materials, from block copolymer films and micelles to polymer nanoparticles of different morphologies. These domains generally have thicknesses on the order of a few nanometers, which are difficult to characterize, but match the typical lengthscale of Förster resonance energy transfer (FRET). In the past, experiments with FRET in nanoheterogeneous polymer materials have been analyzed with empirical models that could only recover qualitative or approximate information. However, using more recent analysis tools which take advantage of the very strong dependence of FRET on the separation distance between donor and acceptor dyes, it is possible to obtain detailed information on the morphology of the nanodomains and the distribution of different components in polymer nanostructured materials. These new tools, or distribution models for FRET, take into account the distribution of donors and acceptors in systems of restricted geometry with planar,[10–12] spherical,[13] or cylindrical[11,20,21,38] symmetry. They have been successfully used in a number of polymer systems with nanodomains and heterogeneous dye concentration profiles, ranging from block copolymer films and micelles[23,65] to polymer nanoparticles,[8,10,66,67] latex film formation,[68,69] and polymer blends.[70]

Although resonance energy transfer has been described by Förster already 60 years ago, only recently have the tools been available to fully explore the nanometer-scale distance dependence of FRET and thus analyze nanostructured polymer materials in detail. We believe these tools can give an important contribution to the booming fields of nanoscience and nanotechnology.

Acknowledgment. We wish to thank Prof. M. A. Winnik for introducing us to the field of FRET in nanodomains. Financial support from FCT (projects POCTI/47885/QUI, POCI/QUI/61054/04 and PTDC/CTM/68451/06) is gratefully acknowledged. Special thanks to Architect Nuno Duarte who designed Figures 1 and 3, and to artist Ana Tristany who painted ″Interfaces″ (steered dripping, acrylic on canvas, 1.5 m x 1.5 m), reproduced in the journal cover.

References and Notes

(1) Bates, F. S. Polymer-Polymer Phase-Behavior. *Science* **1991**, *251* (4996), 898–905.
(2) Forster, T. Experimentelle und Theoretische Untersuchung des Zwischenmolekularen Ubergangs Von Elektronenanregungsenergie. *Z. Naturforsch. Sect. A* **1949**, *4* (5), 321–327.
(3) Forster, T. Zwischenmolekulare Energiewanderung und Fluoreszenz. *Ann. Phys.* **1948**, *2* (1−2), 55–75.
(4) Morawetz, H. Some Applications of Fluorimetry to Synthetic-Polymer Studies. *Science* **1979**, *203* (4379), 405–410.
(5) Baumann, J.; Fayer, M. D. Excitation Transfer in Disordered Two-Dimensional and Anisotropic 3-Dimensional Systems - Effects of Spatial Geometry on Time-Resolved Observables. *J. Chem. Phys.* **1986**, *85* (7), 4087–4107.
(6) Klafter, J.; Blumen, A. Fractal Behavior in Trapping and Reaction. *J. Chem. Phys.* **1984**, *80* (2), 875–877.
(7) Drake, J. M.; Klafter, J.; Levitz, P. Chemical and Biological Microstructures As Probed by Dynamic Processes. *Science* **1991**, *251* (5001), 1574–1579.
(8) Farinha, J. P. S.; Martinho, J. M. G.; Yekta, A.; Winnik, M. A. Direct Nonradiative Energy-Transfer in Polymer Interphases - Fluorescence

Decay Functions from Concentration Profiles Generated by Fickian Diffusion. *Macromolecules* **1995**, *28* (18), 6084–6088.

(9) Yekta, A.; Duhamel, J.; Winnik, M. A. Dipole-Dipole Electronic-Energy Transfer - Fluorescence Decay Functions for Arbitrary Distributions of Donors and Acceptors - Systems with Planar Geometry. *Chem. Phys. Lett.* **1995**, *235* (1−2), 119–125.

(10) Farinha, J. P. S.; Martinho, J. M. G.; Kawaguchi, S.; Yekta, A.; Winnik, M. A. Latex film formation probed by nonradiative energy transfer: Effect of grafted and free poly(ethylene oxide) on a poly(n-butyl methacrylate) latex. *J. Phys. Chem.* **1996**, *100* (30), 12552–12558.

(11) Farinha, J. P. S.; Martinho, J. M. G. Electronic energy transfer in restricted geometries - Application to the study of spherical and planar interphases of diblock copolymer films. *J. Lumin.* **1997**, *72−4*, 914–917.

(12) Yekta, A.; Winnik, M. A.; Farinha, J. P. S.; Martinho, J. M. G. Dipole-dipole electronic energy transfer. Fluorescence decay functions for arbitrary distributions of donors and acceptors 0.2. Systems with spherical symmetry. *J. Phys. Chem. A* **1997**, *101* (10), 1787–1792.

(13) Farinha, J. P. S.; Spiro, J. G.; Winnik, M. A. Dipole-dipole electronic energy transfer: Fluorescence decay functions for arbitrary distributions of donors and acceptors in systems with cylindrical symmetry. *J. Phys. Chem. B* **2004**, *108* (42), 16392–16400.

(14) Bates, F. S.; Fredrickson, G. H. Block copolymers - Designer soft materials. *Phys. Today* **1999**, *52* (2), 32–38.

(15) Stoykovich, M. P.; Nealey, P. F. Block copolymers and conventional lithography. *Mater. Today* **2006**, *9* (9), 20–29.

(16) Fredrickson, G. H.; Bates, F. S. Dynamics of block copolymers: Theory and experiment. *Annu. Rev. Mater. Sci.* **1996**, *26*, 501–550.

(17) Matsen, M. W.; Bates, F. S. Origins of complex self-assembly in block copolymers. *Macromolecules* **1996**, *29* (23), 7641–7644.

(18) Matsen, M. W.; Bates, F. S. Unifying weak- and strong-segregation block copolymer theories. *Macromolecules* **1996**, *29* (4), 1091–1098.

(19) Zhang, L. F.; Eisenberg, A. Multiple Morphologies of Crew-Cut Aggregates of Polystyrene-b-Poly(Acrylic Acid) Block-Copolymers. *Science* **1995**, *268* (5218), 1728–1731.

(20) Schillen, K.; Yekta, A.; Ni, S. R.; Farinha, J. P. S.; Winnik, M. A. Characterization of polyisoprene-b-poly(methyl methacrylate) diblock copolymer micelles in acetonitrile. *J. Phys. Chem. B* **1999**, *103* (43), 9090–9103.

(21) Farinha, J. P. S.; Schillen, K.; Winnik, M. A. Interfaces in self-assembling diblock copolymer systems: Characterization of poly(isoprene-b-methyl methacrylate) micelles in acetonitrile. *J. Phys. Chem. B* **1999**, *103* (13), 2487–2495.

(22) Pichot, C. Surface-functionalized latexes for biotechnological applications. *Curr. Opin. Colloid Interface Sci.* **2004**, *9* (3−4), 213–221.

(23) Farinha, J. P. S.; Charreyre, M. T.; Martinho, J. M. G.; Winnik, M. A.; Pichot, C. Picosecond fluorescence studies of the surface morphology of charged polystyrene latex particles. *Langmuir* **2001**, *17* (9), 2617–2623.

(24) Steinber, I. Z. Nonradiative Energy Transfer in Systems in Which Rotatory Brownian Motion Is Frozen. *J. Chem. Phys.* **1968**, *48*, 2411–2413.

(25) Yang, J.; Winnik, M. A.; Pakula, T. Numerical simulations of fluorescence resonance energy transfer in diblock copolymer lamellae. *Macromolecules* **2005**, *38* (21), 8882–8890.

(26) Dale, R. E.; Eisinger, J.; Blumberg, W. E. Orientational Freedom of Molecular Probes - Orientation Factor in Intra-Molecular Energy-Transfer. *Biophys. J.* **1979**, *26* (2), 161–193.

(27) Isaksson, M.; Norlin, N.; Westlund, P. O.; Johansson, L. B. A. On the quantitative molecular analysis of electronic energy transfer within donor - acceptor pairs. *Phys. Chem. Chem. Phys.* **2007**, *9* (16), 1941–1951.

(28) Berberan-Santos, M. N.; Valeur, B. Fluorescence Depolarization by Electronic-Energy Transfer in Donor-Acceptor Pairs of Like and Unlike Chromophores. *J. Chem. Phys.* **1991**, *95* (11), 8048–8055.

(29) Lewis, F. D.; Zhang, L. G.; Zuo, X. B. Orientation control of fluorescence resonance energy transfer using DNA as a helical scaffold. *J. Am. Chem. Soc.* **2005**, *127* (28), 10002–10003.

(30) Snyder, B.; Freire, E. Fluorescence Energy-Transfer in 2 Dimensions - A Numeric Solution for Random and Nonrandom Distributions. *Biophys. J.* **1982**, *40* (2), 137–148.

(31) Stryer, L; Haugland, R. P. Energy Transfer - A Spectroscopic Ruler. *Proc. Natl. Acad. Sci. U.S.A.* **1967**, *58* (2), 719.

(32) Yang, C. L.; Evesque, P.; Elsayed, M. A. Fractal-Like, But Nonfractal, Behavior of One-Step Dipolar Energy-Transfer on Regular Lattices with Excluded Volume. *J. Phys. Chem.* **1985**, *89* (16), 3442–3444.

(33) Gochanour, C. R.; Andersen, H. C.; Fayer, M. D. Electronic Excited-State Transport in Solution. *J. Chem. Phys.* **1979**, *70* (9), 4254–4271.

(34) Klafter, J.; Blumen, A.; Drake, J. M. *In Molecular Dynamics in Restricted Geometries*; Klafter, J., Drake, J. M., Eds.; Wiley: New York, 1989; pp 1−22..

(35) Levitz, P.; Drake, J. M.; Klafter, J. Critical-Evaluation of the Application of Direct Energy-Transfer in Probing the Morphology of Porous Solids. *J. Chem. Phys.* **1988**, *89* (8), 5224–5236.

(36) Martinho, J. M. G.; Farinha, J. P.; Berberan-santos, M. N.; Duhamel, J.; Winnik, M. A. Test of A Model for Reversible Excimer Kinetics - Pyrene in Cyclohexanol. *J. Chem. Phys.* **1992**, *96* (11), 8143–8149.

(37) Sidorenko, A.; Tokarev, I.; Minko, S.; Stamm, M. Ordered reactive nanomembranes/nanotemplates from thin films of block copolymer supramolecular assembly. *J. Am. Chem. Soc.* **2003**, *125* (40), 12211–12216.

(38) Farinha, J. P. S.; Spiro, J. G.; Winnik, M. A. Energy transfer in the restricted geometry of lamellar block copolymer interfaces. *J. Phys. Chem. B* **2001**, *105* (21), 4879–4888.

(39) Spiro, J. G.; Yang, J.; Zhang, J. X.; Winnik, M. A.; Rharbi, Y.; Vavasour, J. D.; Whitmore, M. D.; Jerome, R. Experimental and theoretical investigation of the lamellar structure of a styrene-butyl methacrylate diblock copolymer by fluorescence resonance energy transfer, small-angle X-ray scattering, and self-consistent-field simulations. *Macromolecules* **2006**, *39* (20), 7055–7063.

(40) Hauser, M.; Klein, U. K. A.; Gosele, U. Extension of Forsters Theory of Long-Range Energy-Transfer to Donor-Acceptor Pairs in Systems of Molecular Dimensions. *Z. Phys. Chem.-Frankfurt* **1976**, *101* (1−6), 255–266.

(41) Wolber, P. K.; Hudson, B. S. Analytic Solution to the Forster Energy-Transfer Problem in 2 Dimensions. *Biophys. J.* **1979**, *28* (2), 197–210.

(42) Dewey, T. G.; Hammes, G. G. Calculation of Fluorescence Resonance Energy-Transfer on Surfaces. *Biophys. J.* **1980**, *32* (3), 1023–1036.

(43) Dewey, T. G.; Hammes, G. G. Calculation of Fluorescence Resonance Energy-Transfer on Surfaces. *Biophys. J.* **1980**, *32* (3), 1023–1036.

(44) Fredrickson, G. H. Intermolecular Correlation-Functions from Forster Energy-Transfer Experiments. *Macromolecules* **1986**, *19* (2), 441–447.

(45) Marquardt, D. W. An Algorithm for Least-Squares Estimation of Nonlinear Parameters. *J. Soc. Ind. Appl. Math.* **1963**, *11* (2), 431–441.

(46) Farinha, J. P. S.; Martinho, J. M. G.; Pogliani, L. Non-linear least-squares and chemical kinetics. An improved method to analyse monomer-excimer decay data. *J. Math. Chem.* **1997**, *21* (2), 131–139.

(47) Helfand, E. Block Copolymers, Polymer-Polymer Interfaces, and Theory of Inhomogeneous Polymers. *Acc. Chem. Res.* **1975**, *8* (9), 295–299.

(48) Helfand, E.; Tagami, Y. Theory of Interface Between Immiscible Polymers 0.2. *J. Chem. Phys.* **1972**, *56* (7), 3592–3601.

(49) Yekta, A.; Spiro, J. G.; Winnik, M. A. A critical evaluation of direct energy transfer as a tool for analysis of nanoscale morphologies in polymers. Application to block copolymer interfaces. *J. Phys. Chem. B* **1998**, *102* (41), 7960–7970.

(50) Yang, J.; Roller, R. S.; Winnik, M. A.; Zhang, Y.; Pakula, T. Energy transfer study of symmetric polyisoprene-poly(methyl methacrylate) diblock copolymers bearing dyes at the junctions: Dye orientation. *Macromolecules* **2005**, *38* (4), 1256–1263.

(51) Yang, J.; Lou, X. D.; Spiro, J. G.; Winnik, M. A. Energy transfer study of the cylindrical interface formed by asymmetric isoprene-methyl methacrylate diblock copolymers bearing a dye at the junction. *Macromolecules* **2006**, *39* (6), 2405–2412.

(52) Rharbi, Y.; Winnik, M. A. Interface thickness of a styrene-methyl methacrylate block copolymer in the lamella phase by direct nonradiative energy transfer. *Macromolecules* **2001**, *34* (15), 5238–5248.

(53) Yang, J.; Lu, J. P.; Rharbi, Y.; Cao, L.; Winnik, M. A.; Zhang, Y. M.; Wiesner, U. B. Energy transfer study of the interface thickness in symmetrical isoprene-methyl methacrylate diblock copolymers. *Macromolecules* **2003**, *36* (12), 4485–4491.

(54) Anastasiadis, S. H.; Russell, T. P.; Satija, S. K.; Majkrzak, C. F. The Morphology of Symmetric Diblock Copolymers As Revealed by Neutron Reflectivity. *J. Chem. Phys.* **1990**, *92* (9), 5677–5691.

(55) Russell, T. P.; Menelle, A.; Hamilton, W. A.; Smith, G. S.; Satija, S. K.; Majkrzak, C. F. Width of Homopolymer Interfaces in the Presence of Symmetrical Diblock Copolymers. *Macromolecules* **1991**, *24* (20), 5721–5726.

(56) Schubert, D. W.; Weidisch, R.; Stamm, M.; Michler, G. H. Interface width of poly(styrene-b-butyl methacrylate) diblock copolymers. *Macromolecules* **1998**, *31* (11), 3743–3745.

(57) Hashimoto, T.; Fujimura, M.; Kawai, H. Domain-Boundary Structure of Styrene-Isoprene Block Co-Polymer Films Cast from Solutions 5. Molecular-Weight Dependence of Spherical Microdomains. *Macromolecules* **1980**, *13* (6), 1660–1669.

(58) Hashimoto, T.; Shibayama, M.; Kawai, H. Domain-Boundary Structure of Styrene-Isoprene Block Co-Polymer Films Cast from Solution 4. Molecular-Weight Dependence of Lamellar Microdomains. *Macromolecules* **1980**, *13* (5), 1237–1247.

(59) Seebergh, J. E.; Berg, J. C. Evidence of A Hairy Layer at the Surface of Polystyrene Latex-Particles. *Colloids Surf. A* **1995**, *100*, 139–153.

(60) Nakashima, K.; Liu, Y. S.; Zhang, P.; Duhamel, J.; Feng, J. R.; Winnik, M. A. Picosecond Fluorescence Studies of Energy-Transfer on the Surface of Poly(Butyl Methacrylate) Latex-Particles. *Langmuir* **1993**, *9* (11), 2825–2831.

(61) Nakashima, K.; Duhamel, J.; Winnik, M. A. Photophysical Processes on A Latex Surface - Electronic-Energy Transfer from Rhodamine Dyes to Malachite Green. *J. Phys. Chem.* **1993**, *97* (41), 10702–10707.

(62) Fidalgo, A.; Farinha, J. P. S.; Martinho, J. M. G.; Rosa, M. E.; Ilharco, L. M. Nanostructured Silica/Polymer Subcritical Aerogels. *J. Mater. Chem.* **2007**, *17*, 2195.

(63) Fidalgo, A.; Farinha, J. P. S.; Martinho, J. M. G.; Rosa, M. E.; Ilharco, L. M. Nanostructured hybrid silica/polymer aerogels dried at ambient pressure. *Chem. Mater.* **2007**, *19*, 2603.

(64) Martinho, J. M. G.; Ilharco, L. M.; Farinha, J. P. S.; Fidalgo, A.; Martinho, P. *Process for the preparation, under subcritical conditions, of monolithic xerogels and aerogels of silica/latex hybrids, modified with alkoxysilane groups*. PCT patent 2007.

(65) Fonseca, T.; Relogio, P.; Martinho, J. M. G.; Farinha, J. P. S. Preparation and surface characterization of polymer nanoparticles designed for incorporation into hybrid materials. *Langmuir* **2007**, *23* (10), 5727–5734.

(66) Ye, X. D.; Farinha, J. P. S.; Oh, J. K.; Winnik, M. A.; Wu, C. Polymer diffusion in PBMA latex films using a polymerizable benzophenone derivative as an energy transfer acceptor. *Macromolecules* **2003**, *36* (23), 8749–8760.

(67) Farinha, J. P. S.; Wu, J.; Winnik, M. A.; Farwaha, R.; Rademacher, J. Polymer diffusion in gel-containing poly(vinyl acetate-co-dibutyl maleate) latex films. *Macromolecules* **2005**, *38* (10), 4393–4402.

(68) Farinha, J. P. S.; Vorobyova, O.; Winnik, M. A. An energy tranfer study of the interface thickness in blends of poly(butyl methacrylate) and poly(2-ethylhexyl methacrylate). *Macromolecules* **2000**, *33* (16), 5863–5873.

(69) Pham, H. H.; Farinha, J. P. S.; Winnik, M. A. Cross-linking, miscibility, and interface structure in blends of poly(2-ethylhexyl methacrylate) copolymers. An energy transfer study. *Macromolecules* **2000**, *33* (16), 5850–5862.

(70) Spiro, J. G.; Farinha, J. P. S.; Winnik, M. A. Thermodynamics and morphology of latex blend films. *Macromolecules* **2003**, *36* (20), 7791–7802.

JP8016437